Astron. Astrophys. 360, 509–519 (2000)

ASTRONOMY
AND
ASTROPHYSICS

Chemical abundances in seven red giants of NGC 2360 and NGC 2447⋆,⋆⋆

S. Hamdani[1], **P. North**[1], **N. Mowlavi**[2], **D. Raboud**[2], **and J.-C. Mermilliod**[1]

[1] Institut d'Astronomie de l'Université de Lausanne, 1290 Chavannes-des-bois, Switzerland
[2] Observatoire de Genève, 1290 Sauverny, Switzerland

Received 6 March 2000 / Accepted 15 June 2000

Abstract. Chemical abundances of about fifteen elements from oxygen to europium are measured in seven red giants of the two open clusters NGC 2360 and NGC 2447. The effective temperatures of the giants are determined spectroscopically by taking advantage of their known masses ($\sim 2\,\mathrm{M}_\odot$ in NGC 2360 and $\sim 3\,\mathrm{M}_\odot$ in NGC 2447) and bolometric magnitudes.

The average iron abundances we obtain for the two clusters are [Fe/H]=0.07 for NGC 2360 and [Fe/H]=0.03 for NGC 2447.

Evolutionary stellar model calculations are performed in the mass range $1-4\,\mathrm{M}_\odot$ in order to analyze the surface Na and O abundances predicted after the first dredge-up. The sodium abundance shows a well defined correlation with stellar mass in the $2-3\,\mathrm{M}_\odot$ range. The agreement between our Na abundance determinations in NGC 2360 and our model predictions at $2\,\mathrm{M}_\odot$ is very good. In contrast, the overabundance in one of the three stars in NGC 2447 exceeds that predicted at $3\,\mathrm{M}_\odot$ by ~ 0.08 dex, which is significant compared to the observational error bars. The effects of core overshooting, convection prescription, metallicity and nuclear reaction rates on the Na surface predictions of our models are investigated.

An oxygen deficiency relative to iron by 0.2 dex is measured in our stars, in disagreement with our model predictions. Assuming that the Sun is 0.1–0.3 dex enriched in oxygen relative to neighbor stars could explain the discrepancy.

Key words: stars: abundances – stars: fundamental parameters – stars: evolution – stars: late-type – Galaxy: open clusters and associations: individual: NGC 2360 – Galaxy: open clusters and associations: individual: NGC 2447

1. Introduction

The comparison of chemical abundances observed at the surface of stars with those predicted by stellar model calculations offers a valuable tool to test our knowledge of stellar evolution. Among the most studied objects are red giants. Those objects are formed after the main sequence (MS) phase when hydrogen has been exhausted in the core. The core contracts, the outer layers expand, and the convective envelope deepens into the core. The consequent mixing of the ashes of hydrogen burning from the deep layers to the surface is called the first dredge-up process (1DUP).

In most cases, the surface abundances after 1DUP are predicted to be sensitive to stellar mass. The observation of red giants belonging to given clusters presents in this respect a unique advantage since the age of the cluster, and thus of its individual stars, is known by comparing the cluster's distribution in the Hertzsprung-Russell diagram with predicted isochrones. The masses of the individual stars are then determined, enabling a thorough comparison of their surface abundances with predictions.

In this paper, we determine the abundances of oxygen, sodium and heavier elements in four red giants of the open clusters NGC 2360 and in three red giants of NGC 2447. All these giants belong to the clumps of their respective clusters. The initial masses of our stars are estimated to 2 and $3\,\mathrm{M}_\odot$ for those in NGC 2360 and NGC 2447, respectively. These masses turn out to be in a critical range for surface sodium enhancement after the 1DUP. Oxygen, on the other hand, is an interesting element to study since it has already been observed to be slightly deficient relative to iron not only in supergiants but also in giants of globular clusters (Brown & Wallerstein 1991) and open clusters (Luck 1994). Finally, the abundances of the iron-group elements are used to directly derive the metallicity of the two clusters. This direct technique, which contrasts with the classical, but less reliable, technique based on color indices and photometric calibrations, has so far been used only in a small number of open clusters (about 20, see Strobel 1991; Twarog et al. 1997). Our observations enable to enlarge that list.

The observational material is presented in Sect. 2 and the abundance determination procedure in Sect. 3. The metallicity is derived in Sect. 4, and the sodium and oxygen abundances analyzed in Sects. 5 and 6, respectively. Conclusions are drawn in Sect. 7.

Send offprint requests to: P. North (pierre.north@obs.unige.ch)

⋆ Based on observations collected at the European Southern Observatory, La Silla, Chile (period 56)

⋆⋆ Table 3 is available only in electronic form at the CDS via anonymous ftp to cdsarc.u-strasbg.fr (130.79.128.5) or via http://cdsweb.u-strasbg.fr/Abstract.html

2. Observational material

Table 1 summarizes some parameters characterizing the two open clusters NGC 2360 and NGC 2447 studied in this paper. The distance modulus has been re-determined using Mermilliod's database (1995, 1999) and the age is determined with the theoretical isochrones of Schaller et al. (1992). They lead to turn-off masses of 1.98 and $2.75\,\mathrm{M}_\odot$ for NGC 2360 and NGC 2447, respectively.

The seven red giants studied in this paper have been selected on the basis of their constant radial velocity, as determined by CORAVEL observations, in order to ensure that they are single stars. This point is important since the light of a secondary component could bias the equivalent widths used to estimate the abundances of the primary.

For each star, one echelle spectrum has been obtained by DR in November 1995 using the EMMI spectrograph attached to the NTT 3.5m telescope at the European Southern Observatory in La Silla, Chile. The grism #5 and the echelle grating #10 were used, yielding spectra in the wavelength range from 4050Å to 6650Å with a resolving power of $R = 28\,000$. The detector was the ESO CCD #36, with 2048×2048 pixels. The signal-to-noise ratio per pixel of the extracted spectra varies from 54 to 226, depending on the wavelength range and exposure time.

The journal of the observations is given in Table 2, together with the main characteristics of each stars (identification, V magnitude, Geneva $[B-V]$ color index, S/N ratio, Julian date, exposure time, radial velocity derived from our spectra and average RV from CORAVEL observations). The radial velocities are determined from our spectra by cross-correlation with a CORAVEL-type binary mask optimized for the K0 spectral type. They are compatible with those determined earlier from CORAVEL observations by Mermilliod & Mayor (1989, 1990), confirming that the red giants of our sample are very probably single.

Observations of two IAU RV standards, HD 66141 and HD 80170 (of which Udry et al. 1999 give the precise RV value from CORAVEL observations), show that our results can be trusted to within ± 1.0 km s^{-1}. To reach this accuracy, we had to monitor the instrumental drift by taking a few short Th-Ar calibration exposures during the night and correlate them with a longer calibration exposure taken in the preceding afternoon; then we linearly interpolated the instrumental velocity shifts for the epochs of the science exposures.

3. Abundance determination

For the reduction of the spectra, we used the Inter-Tacos software of Geneva Observatory[1]. The spectra were divided by an average of six flat-field exposures, after the background had been fitted by 2-d polynomials and subtracted. Then, they were extracted using a simple addition of the intensities along a virtual slit of 15 pixels. The wavelength calibration was performed with the same software, using Th-Ar spectra taken in the afternoon preceding the night. The rms scatter of the residuals around the fitted dispersion relation was 3.1 mÅ, which is quite good for this resolution. After rebinning to a constant wavelength step of 0.03 Å, which is over-sampled, we filtered all spectra by eliminating the high frequencies of their Fourier Transform. For that purpose, we used a FFT with a window of 65% of $\Delta\lambda$ ($\Delta\lambda = \lambda$/R). The 55 orders were individually normalized to the continuum, using an interactive Supermongo procedure which interpolates between the continuum points by a 3rd degree spline.

[1] The Inter-Tacos software is the same as that used for the Elodie and Coralie spectrographs.

Table 1. Adopted parameters for NGC 2360 and 2447, including the iron abundance [Fe/H] and metallicity [M/H] obtained in this paper (Sect. 4). The mass $\mathrm{M}_{\mathrm{turn-off}}$ at the turn-off (defined as point T in Fig. 1 of Maeder & Meynet 1991) is given too.

	NGC 2360	NGC 2447
α (1950)	$7^{\mathrm{h}}15.5^{\mathrm{m}}$	$7^{\mathrm{h}}42.5^{\mathrm{m}}$
δ (1950)	$-15°32'$	$-23°45'$
$m_{\mathrm{V}} - M_{\mathrm{V}}$	10.40	10.25
$E(B-V)$	0.07	0.04
A_{V}	0.22	0.13
Distance [kpc]	1.086	1.057
Log Age	9.06	8.65
$\mathrm{M}_{\mathrm{turn-off}}$ [$\mathrm{M}_\odot$]	1.98	2.75
[Fe/H]	0.07	0.03
[M/H]	0.10	0.05

3.1. Abundance determination

The list of lines and oscillator strengths used for our abundance determinations is the same as that adopted by Boyarchuk et al. (1996). The photospheric lines are chosen in wavelength zones avoiding the telluric absorption lines. The equivalent widths below 10 mÅ are rejected because they are too sensitive to noise and normalization. Table 3 (available only in electronic form) summarizes the line parameters and measured equivalent widths. For Mg I, not included in the list of Boyarchuk et al., we adopt the $\log gf$ values of Thévenin (1989, 1990).

The abundances are determined using the MOOG code (C. Sneden, Texas University) in the "abfind" mode, combined with atmospheric models of Kurucz (1996). The Kurucz models are interpolated by cubic splines in the T_{eff} and $\log g$ plane (solar abundances are assumed as far as the atmospheric structure is concerned). For some lines for which we have reasons to suspect that blends would make the equivalent width method risky (oxygen and europium), we compute a synthetic spectrum including a large number of neighboring lines, and determine the abundance of the considered element by best fitting the synthetic spectra to the observed one (the 'best' fit being evaluated by eye estimate). In that case, the MOOG code is used in its "synth" mode and the lines are taken from the VALD database (Piskunov et al. 1995).

The measurement of abundance deviations as small as 0.15 dex requires good spectra with signal-to-noise (S/N) ratios above 100. Such a S/N is reached at almost all wavelengths

Table 2. Observational data of the 7 red giants and signal-to-noise ratio per pixel of their extracted spectra. The V magnitude and $[B-V]$ index are those of Geneva photometry. The adopted numbering is that of Becker et al. (1976), but we also give the numbers in the system of Eggen (1968) for NGC 2360. There is no other numbering system for NGC 2447, but the map of this cluster is available on the web (Mermilliod 1999).The radial velocities of the 7 red giants and of two reference stars are also given, as determined in this work ("EMMI") at the indicated Julian dates. The exposure times are also listed. The CORAVEL RV values ("COR.") of the cluster stars are average ones from Mermilliod & Mayor (1989, 1990), while those of the reference stars (IAU standards) are taken from Udry et al. (1999). The errors quoted for the CORAVEL observations are related to the average RV values; the last column ("N") gives the number of CORAVEL measurements.

Star	DM or Eggen No	V	[B-V]	S/N ratio around 5150Å	S/N ratio around 6600Å	JD -2450000	t_{exp} [s]	V_r [km s^{-1}] EMMI	V_r [km s^{-1}] COR.	N COR.
2360-7	8	11.087	0.294	54	89	30.741	1800	28.53	27.2±0.2	5
2360-50	67	11.082	0.311	71	108	30.767	2700	27.65	27.2±0.3	4
2360-62	81	11.272	0.251	73	146	31.730	3600	28.05	27.3±0.5	4
2360-86	110	10.787	0.309	114	181	31.822	3600	26.72	27.3±0.3	4
2447-28	-23° 6102	9.849	0.226	112	170	30.847	1800	19.98	21.2±0.2	3
2447-34		10.123	0.197	143	236	32.755	3000	23.30	22.1±0.2	3
2447-41		10.031	0.204	124	226	32.840	2700	21.40	21.5±0.2	3
HD 66141	HR 3145	4.406	0.637			30.833	90	71.43	71.6±0.3	
						33.827	90	73.10		
HD 80170	HR 3694	5.310	0.510			31.799	180	1.38	0.5±0.2	

in all our spectra, except near the [O I] line in three stars in NGC 2360 (star numbers 7, 50 and 62). No O abundance is presented for those stars.

3.2. Atmospheric parameters

The determination of the atmospheric parameters $\log g$ (gravity), $T_{\rm eff}$ (effective temperature) and $V_{\rm t}$ (microturbulent velocity) is crucial for a good abundance estimation. The fact that the distance to the open clusters and the masses M of the individual stars are known provides a relation between $\log g$ and T_{eff} given by

$$\log g = -12.51 + \log M + 4\log T_{\rm eff} + 0.4(M_{\rm V} + BC), \quad (1)$$

where M is expressed in solar mass, $M_{\rm V}$ is the absolute visual magnitude in V and BC is the bolometric correction. We assume $M_{\rm bol\odot} = 4.75$, and take the bolometric corrections from Flower (1977) (which are very close to the theoretically derived ones of Bessell et al. 1998).

The atmospheric parameters $T_{\rm eff}$ and $V_{\rm t}$ of each star are estimated from an iterative procedure based on the method used by Boyarchuk et al. (1996), but modified to take into account the known bolometric magnitudes of the stars.

Let us consider a given star. Starting with an initial guess of $V_{\rm t} = 1.6$ km s^{-1}, we construct a diagram (Fig. 1) plotting the abundances of the iron-peak elements computed by MOOG from our observed spectrum, as a function of the effective temperature ($\log g$ is computed for each $T_{\rm eff}$ value through Eq. 1). If all iron-peak elements had a solar abundance distribution, then there should be a value of $T_{\rm eff}$ at which their abundances (normalized to solar) are identical. In practice, we choose (by visual estimate) the value of $T_{\rm eff}$ at which the spread of abundances is minimal. Then, for this $T_{\rm eff}$ value, the usual diagram showing the Fe I abundances versus equivalent widths is used to adjust the best velocity of microturbulence $V_{\rm t}$. Finally, the whole procedure is reiterated in order to get mutually consistent parameters.

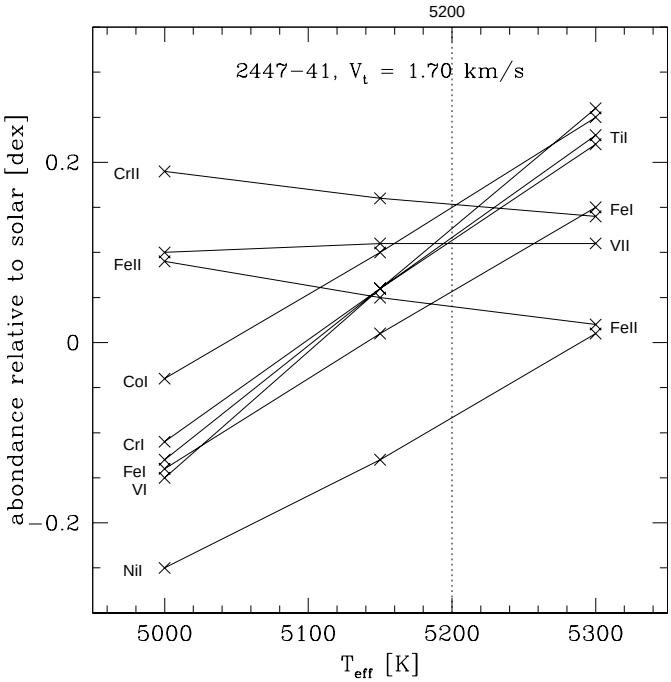

Fig. 1. Abundances of the iron-group elements as a function of effective temperature for the star NGC 2447-41. The value of $\log g$ is given by Eq. 1 at each effective temperature. The vertical line shows the adopted $T_{\rm eff}$ value.

The value of $V_{\rm t}$ found after the convergence of the iterative procedure differs by no more than 0.15 km s^{-1} with the first guess, which is consistent with the formal standard deviation of 0.11 km s^{-1} for that parameter, obtained from the uncertainty on the regression line of Fe I abundances versus equivalent widths.

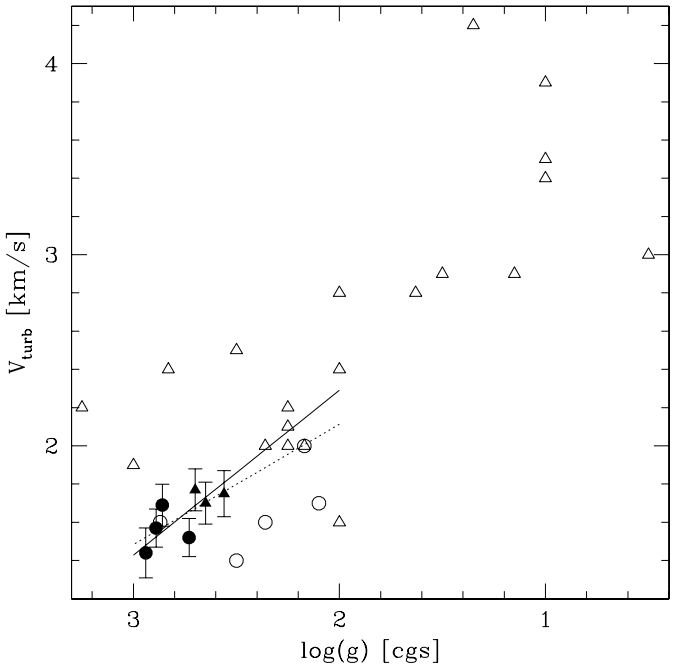

Fig. 2. Microturbulent velocity as a function of surface gravity. Full dots: NGC 2360; full triangles: NGC 2447; open dots: field giants of Boyarchuk et al. (1996); open triangles: cluster giants and supergiants of Luck (1994) with $4500 \leq T_{\rm eff} \leq 5500$ K. Full line: regression line fitted to our seven stars assuming the same error on both axes; dotted line: regression line assuming no error on the abscissa.

This iterative procedure is applied to each of our stars. The resulting atmospheric parameters are summarized in Table 4. The derived effective temperatures agree to better than 100 K with the classical one based on the lack of correlation between abundance and excitation potential, the agreement improving with S/N ratio.

Finally, the sensitivity of our abundance determinations to the adopted atmosphere models is tested by recomputing some abundances with the models of Bell et al. (1976). They lead to similar results, in the sense that abundances given by individual lines are the same within ± 0.07 dex after allowance for a slight systematic offset: the models of Bell et al. systematically lead to a 0.04 dex underabundance compared to Kurucz's models (for lines with an equivalent width $W_\lambda < 100$ mÅ; the offset is larger for stronger lines). In view of the relatively good agreement between both sets of models, we chose the Kurucz ones because they are more recent and easier to use.

The surface abundance of a given element is determined by adjusting the equivalent width(s) of its line(s) predicted by synthetic spectra to those measured in the observed spectra. Actually the MOOG program computes an abundance for each line of a given element, and derives a mean abundance value by averaging the abundances associated to each of those lines. In computing the synthetic spectra, the formation of a dozen molecules (among them C_2, CH, CN, CO, MgH, TiO) is considered.

In the case of Eu, the only usable line is blended. We therefore determine its abundance by a visual match on a synthetic spectrum which includes all possible blends. This element is marked with an asterisk in Table 3. The same technique is used for oxygen, discussed in Sect. 6. The $\lambda 6645.1$ Eu II line does not seem to be significantly affected by hyperfine structure, since its equivalent width in the Sun provides an abundance perfectly consistent with the meteoritic one, using precise experimental oscillator strengths (Biémont et al. 1982). Our $\log gf$ value adopted for this line is only 0.03 dex below the one used by Biémont et al., so it would lead to a solar Eu abundance of 0.53 instead of 0.50 dex, while the meteoritic abundance is 0.54 ± 0.01 dex (Grevesse & Noels 1993).

The elemental abundances found in this work are listed in Table 4.

3.3. $V_{\rm t}$ *versus* $\log g$

For information, we plot in Fig. 2 (filled circles and triangles) the microturbulence velocity deduced for our stars as a function of the surface gravity, together with the measurements of Boyarchuk et al. (1996) for five G7-K0 field giants (open circles, their sixth star is not considered because it is much cooler, of M0 type) and those of Luck (1994) for clusters' supergiants and giants with $4500 \leq T_{\rm eff} \leq 5500$ K (open triangles). The combined data reveals a positive correlation between $V_{\rm t}$ and $\log g$.

Considering only our seven points, the usual correlation coefficient $\rho = -0.697$ gives a t-test value of only -2.17, implying a significance level of about 90 percent, while the Spearman rank correlation coefficient $\rho_{\rm Spearman} = -0.786$ gives a slightly better t-test of -2.84 and a significance level of 96 percent. For the usual LSQ fit assuming no error on the abscissa and a constant error on the ordinate, we find

$$V_{\rm t} = (-0.63 \pm 0.29) \log g + (3.37 \pm 0.80) \quad (2)$$

with an rms scatter of the residuals of 0.083 km s^{-1}. For a fit where errors are assumed to be the same on both axes, the relation would be

$$V_{\rm t} = -0.86 \log g + 4.01 \quad (3)$$

with an rms scatter of the residuals of 0.088 km s^{-1}. The scatter of the residuals is entirely compatible with the internal standard deviation of $V_{\rm t}$ given above. It is smaller than that of the data from Luck (1994) and from Boyarchuk et al. (1996), partly due to the better homogeneity in metallicity and effective temperature.

4. Metallicity

It is difficult to derive an error estimate on the abundances. If we assume that each star has a solar distribution of heavy elements, then an error estimate is given by the dispersion of the heavy element abundances around the mean abundance (relative to solar). The abundances of all measured elements are shown in Fig. 3 for each of our stars, with the mean iron-peak element abundance indicated by a dashed line in each panel. From visual inspection (and excluding Ni which seems underabundant

Table 4. Fundamental parameters of the 7 red giants and mean abundances relative to the Sun. For each species, the second line gives the rms standard deviation of the abundances obtained from individual lines. N is the number of lines measured. The oxygen abundances and [O/Fe] are derived from the equivalent width neglecting the possible contribution of the Ni I $\lambda 6300.33$ line, while [O/Fe]* is computed from a synthetic spectrum including the Ni I $\lambda 6300.33$ line (with the gf value from Kurucz 1994). [Fe/H] is an average weighted by the number of Fe I and Fe II lines. [M/H] is a similar average, but on all iron-peak elements from Ca to Ni.

	2360-7		2360-50		2360-62		2360-86		2447-28		2447-34		2447-41	
Mass [$M_\odot$]	2.10		2.10		2.08		2.13		2.93		2.81		2.87	
$M_{\rm bol}$	0.51		0.49		0.68		0.18		-0.60		-0.30		-0.40	
$M_{\rm V}$	0.69		0.68		0.87		0.39		-0.40		-0.13		-0.22	
$T_{\rm eff}$	5230		5170		5180		5130		5140		5250		5200	
$\log g$	2.89		2.86		2.94		2.73		2.56		2.70		2.65	
$V_{\rm t}$	1.57		1.69		1.44		1.52		1.75		1.77		1.70	
	N	[El./H]	N	[El./H]	N	[El./H]	N	[El./H]	N	[El./H]	N	[El./H]	N	[El./H]
O I							1	-0.07	1	-0.11	1	-0.16	1	-0.22
Na I	2	0.23	2	0.15	2	0.16	2	0.15	2	0.21	2	0.20	2	0.23
		0.01		0.04		0.00		0.03		0.00		0.00		0.01
Mg I	2	0.14	2	0.04	2	0.11	2	0.03	2	0.07	2	0.04	2	0.03
		0.00		0.04		0.03		0.06		0.03		0.08		0.06
Si I	7	0.08	7	0.01	7	0.04	7	0.02	6	0.05	7	-0.01	7	0.06
		0.09		0.09		0.07		0.06		0.13		0.09		0.09
Ca I	9	0.20	9	0.11	9	0.15	9	0.14	9	0.01	9	0.06	9	0.07
		0.11		0.12		0.08		0.08		0.16		0.13		0.11
Sc II	2	0.08	1	0.03	2	0.15	2	0.13	2	-0.07	2	0.03	2	0.07
		0.05				0.09		0.07		0.16		0.02		0.03
Ti I	8	0.16	9	0.13	9	0.14	9	0.11	8	0.06	9	0.18	9	0.11
		0.13		0.16		0.17		0.16		0.18		0.16		0.25
V I	7	0.27	6	0.16	7	0.19	5	0.16	6	0.05	6	0.16	6	0.13
		0.16		0.11		0.16		0.09		0.05		0.10		0.16
V II	1	0.33					1	0.22	2	0.15	1	0.19	2	0.11
										0.07				0.08
Cr I	18	0.23	17	0.12	16	0.16	17	0.12	16	0.08	16	0.12	16	0.11
		0.20		0.20		0.18		0.16		0.17		0.15		0.18
Cr II	4	0.23	3	0.14	4	0.20	4	0.22	3	0.14	3	0.13	3	0.15
		0.04		0.06		0.07		0.10		0.20		0.15		0.11
Fe I	57	0.15	55	0.01	52	0.08	55	0.04	55	-0.01	56	0.05	57	0.05
		0.17		0.17		0.17		0.16		0.21		0.19		0.19
Fe II	4	0.15	4	0.11	4	0.16	4	0.04	4	0.06	4	0.03	4	0.04
		0.10		0.20		0.17		0.13		0.16		0.13		0.16
Co I	6	0.31	7	0.17	7	0.14	7	0.16	8	0.15	9	0.15	9	0.15
		0.28		0.28		0.24		0.30		0.25		0.17		0.24
Ni I	11	0.07	11	-0.10	10	-0.04	11	-0.09	11	-0.09	11	-0.05	11	-0.09
		0.08		0.16		0.12		0.18		0.20		0.18		0.19
Y II	2	0.10	2	0.04	2	0.10	2	-0.03	2	-0.03	2	-0.01	2	-0.02
		0.09		0.08		0.03		0.08		0.03		0.11		0.06
Ce II	2	0.22	2	0.19	2	0.19	2	0.16	2	0.07	2	0.12	2	0.09
		0.04		0.12		0.14		0.24		0.00		0.02		0.01
Eu II	1	0.08			1	0.04	1	0.08	1	0.05	1	0.02	1	0.01
[Na/Fe]		0.08		0.13		0.07		0.11		0.22		0.15		0.18
[O/Fe]								-0.11		-0.12		-0.21		-0.27
[O/Fe]*						~ -0.6		-0.72		-0.54		-0.60		-0.72
[Fe/H]		0.15		0.02		0.09		0.04		-0.01		0.05		0.05
[M/H]		0.18		0.06		0.11		0.07		0.02		0.08		0.07

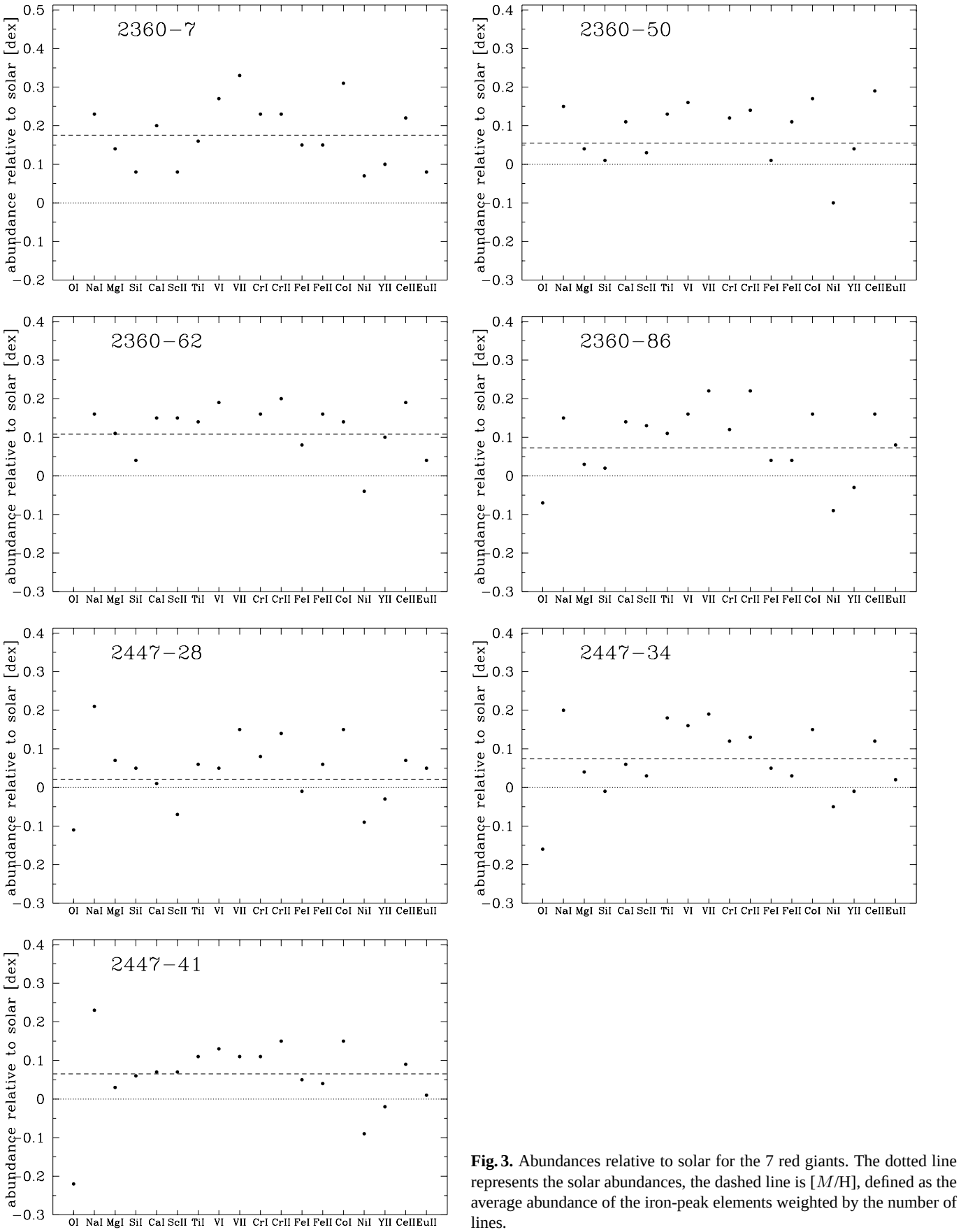

Fig. 3. Abundances relative to solar for the 7 red giants. The dotted line represents the solar abundances, the dashed line is [M/H], defined as the average abundance of the iron-peak elements weighted by the number of lines.

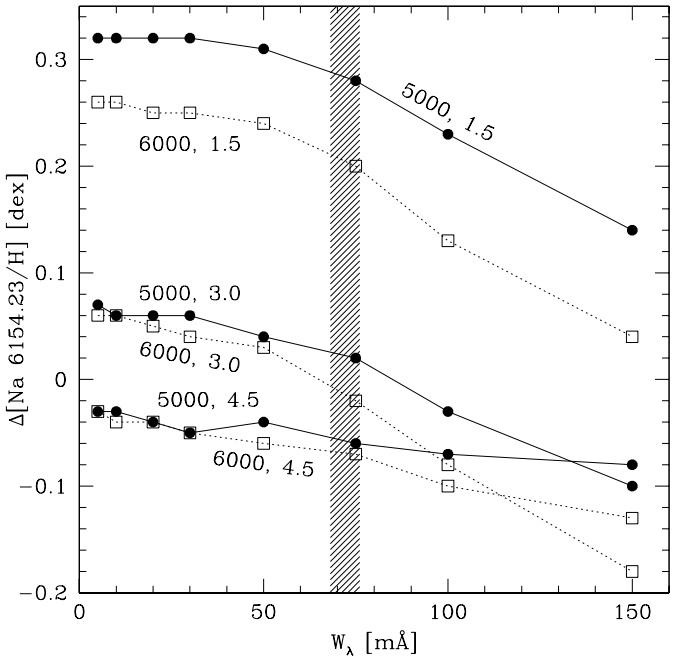

Fig. 4. NLTE effects on the Na I $\lambda 6154.22$ line according to Gratton et al. (1999). Full dots linked with continuous curves are for models with $T_{\rm eff} = 5000$ K and the three surface gravities $\log g = 1.5, 3.0, 4.5$. Open squares linked with dotted lines: $T_{\rm eff} = 6000$ K and same $\log g$ values. The metallicity is solar ([M/H]=0.0) in all cases. The shaded area defines the range of equivalent widths observed in our sample of seven giants.

in some of our stars, probably only because of some systematic error in the oscillator strengths), we estimate the error on the abundance of a given element to be ± 0.1 dex. Table 4 summarizes the abundances derived in all our stars together with the number of lines used for their determination.

The metallicity of each star is defined as a weighted average of the abundances of the iron-group elements, the weight being the number of lines. Since these weights are roughly the same for all stars, each cluster's metallicity is defined as the arithmetic mean of the metallicities of its stars. The values found are [M/H]=0.10 for NGC 2360 and [M/H]=0.05 for NGC 2447. The iron abundances are slightly smaller: [Fe/H]=0.07 for NGC 2360 and [M/H]=0.03 for NGC 2447. Those are reported in Table 4.

5. Sodium

5.1. Abundances

The sodium overabundances [Na/Fe] derived from our spectra are summarized in Table 4 for our seven stars. They are small in NGC 2360, the oldest of the two clusters, with [Na/Fe]= 0.07 – 0.13 dex, and amount to 0.15 – 0.22 dex in NGC 2447.

The error in the Na overabundance [Na/Fe] due to the uncertainties on $T_{\rm eff}$, $\log g$ and $V_{\rm t}$ are not large because Na I and Fe I have similar behaviors with respect to those parameters (e.g. Table 9 of Luck 1994) such that their effect on the [Na/Fe] ratio cancels out. The errors on the [Na/Fe] ratio due to the continuum placement, on the one hand, and to the photon noise, on the other hand, are estimated in the following way. For each star, the equivalent widths of the two Na I lines are measured five times, each time after having renormalized the spectrum of the relevant region. The standard deviations of the equivalent widths are then computed from these data and propagated into standard deviations of abundances using the MOOG code. The resulting dispersion on the Na abundance amounts to 0.02–0.05 dex, depending on the S/N ratio. A synthetic spectrum of a typical red giant (with $T_{\rm eff} = 5200$ K, $\log g = 2.77$, [M/H]=0.0 but [Na/Fe]=+0.15) is then produced, and a Gaussian noise added to it for four representative S/N values, five spectra being produced independently with the same S/N ratio. The equivalent widths of both Na lines are measured (by a Gaussian fit) for these 20 spectra and their standard deviation computed for each S/N ratio. The deviations are found to lie between 2 and 3.3 percent for S/N ratios between 230 and 90. They are translated into abundance errors (after dividing them by $\sqrt{2}$ since there are two lines) and added quadratically to the errors due to the continuum position. Finally, we assume that the error on the continuum position for Fe I is similar to that for Na I and, admitting that they are independent of each other, add them quadratically to the total error on the Na abundance[2] (in fact there is probably a correlation between the continuum placement for the Fe lines and that for the Na lines, but neglecting it only results in an overestimate of the error, so that we stay on the safe side). The resulting estimated errors amount to about 0.03–0.07 dex, the lowest ones pertaining to NGC 2447.

Among the systematic errors which may affect the Na and Fe abundances, some are negligible for the [Na/Fe] abundance ratio because of their mutual cancelation, as mentioned above. This is not the case, however, for the oscillator strengths adopted in the synthetic spectra. If the $\log gf$ values of the two Na I lines are slightly in error while those of Fe I are statistically correct, for instance, then the absolute values of [Na/Fe] would be wrong, though their relative values (i.e. their differences) would remain valid.

Finally, let us consider the systematic errors due to the assumption of local thermodynamic equilibrium (LTE) in the MOOG program. Non-LTE (NLTE) calculations performed by Gratton et al. (1999) in atmospheric conditions relevant to red giants show that the NLTE effect on the Na I $\lambda 6154.22$ line (one of the two lines used in this paper) strongly depends on surface gravity and slightly on effective temperature. This is illustrated in Fig. 4, which reveals that the NLTE correction should be small in the $2.5 < \log g < 3$ range characterizing our stars. Indeed, the average NLTE corrections are found to amount to 0.006–0.035 dex for the stars in NGC 2360 and of 0.032–0.048 dex for NGC 2447 using Table 11 of Gratton et al. (quadratically interpolated in $\log g$ and linearly in $T_{\rm eff}$, and assuming similar corrections for both $\lambda 6154.22$ and $\lambda 6160.75$ lines of

[2] the error on the Fe abundance due to photon noise is neglected because of the large number of lines of this element

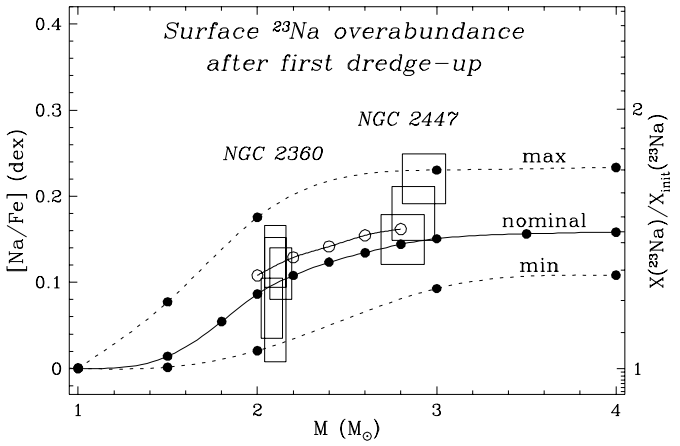

Fig. 5. Na overabundance versus stellar mass. The rectangles represent the abundance determined in our seven red giants with the estimated error bars. The theoretical curves are obtained at metallicity [Z=0.05]. The continuous line joining the full dots is obtained with standard reaction rates and without overshooting, while that joining the open dots takes overshooting into account. The dotted lines show the predictions of a standard model (without overshooting) with extreme reaction rates still compatible with the uncertainties.

Na I). A similar calculation for iron[3] leads to NLTE corrections for Fe of 0.015–0.021 dex for NGC 2360 and 0.027–0.028 dex for NGC 2447. The resulting NLTE effects on [Na/Fe] thus ranges between -0.013 and 0.014 dex for NGC 2360 and between 0.005 and 0.020 for NGC 2447. Of course, these values are only approximate since they are derived from only one iron line assumed to be representative of the 55 lines observed for that element, but they do suggest that the errors brought by our LTE approximation are much smaller than the above mentioned random error bars.

As a conclusion, the main abundance errors, besides the possible systematic errors due to the oscillator strengths[4], are due to the equivalent width and continuum measurements, which amount up to 0.07 dex. The error bars on the masses of each star, on the other hand, are estimated by considering a 0.05 dex error on the age $\log t$ of the clusters. The surface sodium overabundances as a function of stellar mass are shown in Fig. 5 by rectangles taking into account the above mentioned uncertainties.

5.2. Predictions

Sodium production during H-burning results from the transformation of $^{22}\mathrm{Ne}$ into $^{23}\mathrm{Na}$ by proton capture. This reaction occurs very efficiently at the temperatures characterizing the core of MS stars (see Appendix A of Mowlavi 1999). First dredge-up then mixes some of the synthesized Na from the deep layers to the surface. This scenario is confirmed by the observation of sodium overabundances at the surface of many giants and supergiants (e.g. Luck 1994; Boyarchuk et al. 1996; Takeda & Takada-Hidai 1994).

The surface Na overabundance predicted by stellar model calculations (without core overshooting) as a function of stellar mass is shown in Fig. 5 by filled circles connected with solid line. The models have a metallicity 0.05 dex above solar (which is the metallicity of NGC 2447) and are followed from the pre-MS up to the completion of the 1DUP. The stellar evolution code is the same as in Mowlavi (1999), except that the NACRE reaction rates (Arnould et al. 1999) are used to follow the nucleosynthesis and that the formalism of Canuto et al. (1996) is used to describe the energy transport in convective zones. The surface sodium abundance is seen to be very sensitive to stellar mass in the $1.5 - 3\,\mathrm{M}_\odot$ range. It increases from no Na enhancement below $\sim 1.5\,\mathrm{M}_\odot$ to an overabundance of 0.15 dex at $\sim 3\,\mathrm{M}_\odot$, and keeps this value for stellar masses up to $6\,\mathrm{M}_\odot$ before increasing again with stellar mass (see, e.g., Mowlavi 1998).

The sensitivity of those predictions to core overshooting, convection prescription and stellar metallicity is explored by computing extra models from the pre-MS to the 1DUP. None of those parameters, however, turns out to have a significant impact on the surface Na abundance. Models with core overshooting (with an extra-mixing extent of 0.20 times the pressure scale at the core boundary) predict a 0.02 dex enhancement (open circles connected with solid line in Fig. 5) compared to predictions without core overshooting. Increasing the metallicity by 0.17 dex does not change the surface [Na/Fe] prediction after 1DUP by more than 0.01 dex. And using the mixing length theory (with a mixing length of 1.5 times the pressure scale height) instead of the Canuto, Goldmann & Mazzitelli formalism does not change the surface abundance predictions within 0.001 dex.

Let us now explore the uncertainties linked to nuclear reaction rates. Both the $^{22}\mathrm{Ne}\,(\mathrm{p}\,,\gamma)\,^{23}\mathrm{Na}$ and p-capture reactions on $^{23}\mathrm{Na}$ are still subject to large uncertainties (Arnould et al. 1999). In order to assess their impact on our surface Na abundance predictions, several models are recomputed from the pre-MS up to the 1DUP with the upper/lower limits for the rates provided by the NACRE compilation (cf. Arnould et al.), as appropriate to minimize/maximize $^{23}\mathrm{Na}$ production. The results in the 'minimal' and 'maximal' $^{23}\mathrm{Na}$ production cases are shown in filled circles connected with dotted lines in Fig. 5. They reveal a variation in the surface Na abundance predictions of up to 0.08 dex relative to the 'nominal' case where the recommended NACRE rates are used. Nuclear reaction rate uncertainties thus dominate the uncertainties associated with stellar metallicity and convection prescriptions for sodium predictions in red giants.

5.3. Discussion

Fig. 5 shows a very good agreement between our Na abundance predictions in $2\,\mathrm{M}_\odot$ model stars and those observed in

[3] We take the theoretical Fe I high excitation line ($EP = 4.1$ eV) with $W_\lambda = 60$ mÅ (Gratton et al. 1999) as representative of our data. Taking the low excitation line ($EP = 0.0$ eV) or $W_\lambda = 90$ mÅ would not change the results for the NLTE corrections.

[4] The $\log gf$ values of the Na I lines given by Boyarchuk et al. (1996) are 0.05 dex higher than those of Thévenin (1990), but 0.04 dex lower than those of Wiese et al. (1969); this suggests that the systematic error on the $\log gf$ values – hence on the abundances – cannot be much larger than 0.05 dex. This is consistent with the error estimate of Thévenin.

NGC 2360. The nominal predictions of the $3\,M_\odot$ model star, on the other hand, seem a little too low compared to the abundances observed in NGC 2447. The predictions in the maximal case of ^{23}Na production would fit the highest Na abundance measured among the three stars observed in NGC 2447. Those predictions, however, would not be compatible with the Na abundances measured in the $2\,M_\odot$ red giants of NGC 2360. Fig. 5 thus suggests that the nominal Ne–Na reaction rates should not be too much altered, if at all. The solution to the discrepancy between our observed Na abundance observations in NGC2447 and predictions should be found in other(s) mechanism(s) such as, possibly, meridional mixing induced by stellar rotation. Further theoretical and observational investigations should be performed before being able to draw a firm conclusion.

Finally, let us mention that the positive sodium abundance – stellar mass correlation translates, at a given effective temperature into a sodium abundance – surface gravity anti-correlation (or sodium abundance – luminosity correlation). This is well known in the literature, and shown in Fig. 6 where our data are displayed together with those of Luck (1994) and Boyarchuck et al. (1996). The dependence on effective temperature is small (Luck 1994). The computation of our 2.2 to $2.8\,M_\odot$ models with core overshooting is carried on up to the clump in the core helium burning phase. The clump is defined as the point where the stellar luminosity (gravity) reaches its minimum (maximum) value after core helium ignition. The sodium abundance (which is not altered between the 1DUP and the clump) predictions for those clump models are shown by a solid line in Fig. 6.

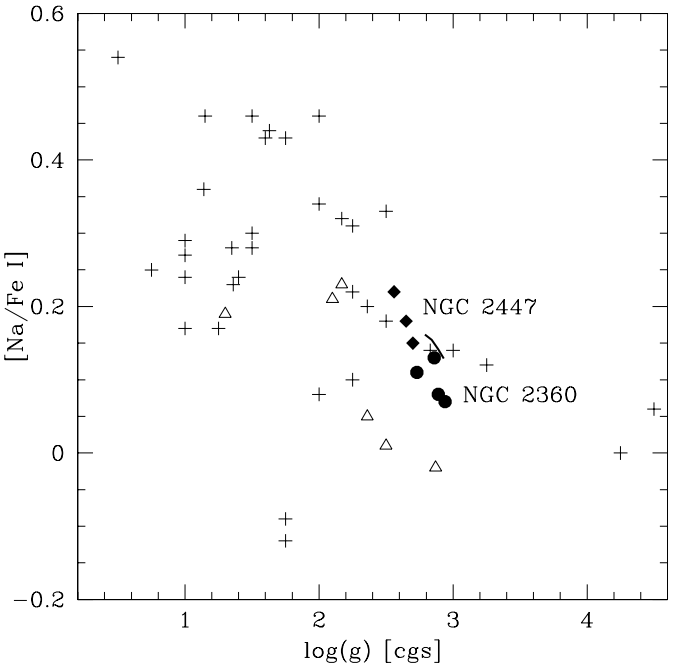

Fig. 6. Na overabundance versus $\log g$. The crosses represent yellow supergiants and giants in clusters measured by Luck (1994), the open triangles represent red giants measured by Boyarchuk et al. (1996) and the full symbols represent the seven red giants of this study (full dots: NGC 2360, full diamonds: NGC 2447). The two crosses at high $\log g$ are dwarfs, while the two supergiants with a negative [Na/Fe] value are among the coolest in Luck's sample ($T_{\rm eff} = 4000$ K). The short solid line on the right of our observations corresponds to predictions of clump stars of 2.2 to $2.8\,M_\odot$ computed with core overshooting.

6. Oxygen

6.1. Abundances

The O abundance is determined from the 6300.31Å line of O I, which is available in our spectra with a S/N ratio above 100 only for the stars of NGC 2447 and for one of the stars in NGC 2360. This line is slightly blended with a line of Sc II at 6300.68Å, but both lines are fairly well separated in our spectra (see Fig. 8). Fortunately, no significant telluric line is spoiling the O and Sc lines, though some are present 1 Å away or more. Using the equivalent width of the 6300.31Å line, the O abundance is found to be slightly deficient with respect to iron, with [O/Fe]$= -0.1$ to -0.3 dex (see Table 4).

The O I line at 6300.31Å, however, may be blended with another line at 6300.33Å from Ni I. The $\log gf$ of the Ni I line is still poorly known. If we take the only data available in the recent literature, i.e. $\log gf = -1.737$ and $EP = 4.266$ eV proposed by Kurucz (1994), and if we assume [Ni/Fe]=0.00, then the oxygen abundance predicted by synthetic spectra reaches -0.6 dex on average (cf. [O/Fe]* in Table 4). A smaller value of $\log gf$ is however suggested from the analysis of the solar spectrum. Lambert (1978) estimates the width W_λ of the Ni I $\lambda 6300.33$ Å line in the solar spectrum to be below 0.1 – 0.5 mÅ. The oscillator strength derived from the solar Ni abundance would be ten times smaller than Kurucz's even with $W_\lambda = 0.5$ mÅ. The true $\log gf$ of this Ni I line is thus very probably smaller than -2.74 dex. Therefore, the blend cannot affect the oxygen abundance determination by more than a few hundredths of dex.

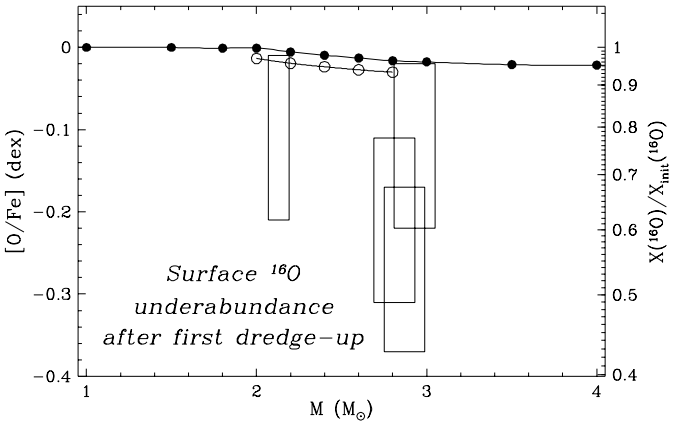

Fig. 7. Same as Fig. 5, but for oxygen.

6.2. Predictions

The surface O underabundance predictions after the first dredge-up are shown in Fig. 7 as a function of stellar mass. Models with (open circles) and without (filled circles) core overshooting during MS both predict very little variation of the surface

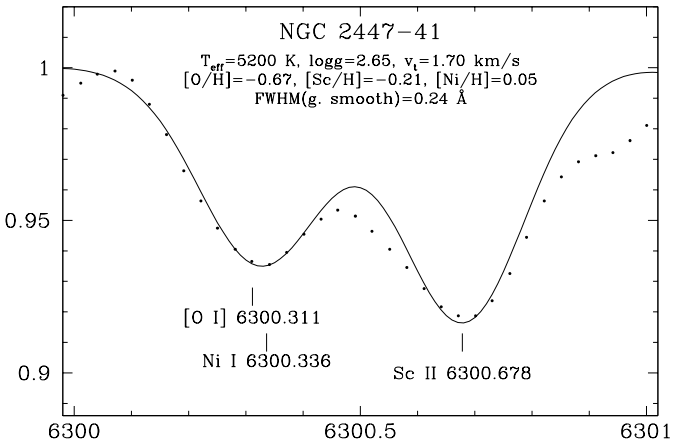

Fig. 8. Measured spectrum of the star NGC 2447-41 (dots), showing how the [O I] line used for the abundance determination is slightly blended with an Sc II line. The continuous line is the synthetic spectrum computed with MOOG, including the [O I] 6300, Sc II and Ni I lines. The abundances adopted for the fit are given on the plot. The measured spectrum has been slightly smoothed using the Fourier method, with a window of 0.15 Å.

O abundance in red giants (depletion by less than 0.04 dex). This results from the fact that only the deepest stellar layers are affected by the N–O cycle of H-burning. As a result, the dilution factor of the envelope's oxygen is rather small when the envelope extends down to the inner regions.

6.3. Discussion

The predicted surface O underabundances fall much below the observed ones (by 0.1 – 0.3 dex). This discrepancy is unexplained so far.

Such a deficiency of O in red giants has already been reported in the literature (e.g. Luck 1994). Interestingly, Venn (1999) argues that the Sun presents an overabundance of oxygen of about 0.3 dex relative to the galactic A supergiants, to B stars in the solar neighborhood and in Orion, and to nebular abundances in the Orion nebula. The conclusion that the solar oxygen abundance is higher than what should be expected by galactic chemical evolution is also reached, at least qualitatively, from the sample of G dwarfs of Edvardsson et al. (1993), which show an average oxygen abundance of [O/Fe]$\sim$-0.1 at [Fe/H]$>$-0.1. If this empirical fact is confirmed, it would explain in a simple way the oxygen underabundances found in our giants, at least if we neglect the contribution of the Ni I line in the synthetic spectra.

7. Conclusions

The abundances of about fifteen elements in seven red giants of NGC 2360 and NGC 2447 are derived with a global uncertainty of about ± 0.1 dex (essentially due to photon noise, normalization of the spectra and uncertainties related to atomic line parameters). From those abundances, the following conclusions are drawn.

The metallicity [M/H] of the two open clusters is directly derived from their iron-group elements. It amounts to 0.10 for NGC 2360 and 0.05 for NGC 2447.

The sodium abundance reveals a positive correlation with stellar mass in the $2-3\,\mathrm{M}_\odot$ range, as expected from model predictions. Quantitatively, the surface ^{23}Na abundances are in good agreement with those predicted after 1DUP for $2\,\mathrm{M}_\odot$ stars (i.e. for stars in NGC 2360), but not at $3\,\mathrm{M}_\odot$ (NGC 2447). The disagreement in NGC 2447 reaches 0.08 dex, which we consider marginally significant given our estimated uncertainties on the Na abundances. The excess of Na observed in two of our stars of NGC 2447, if confirmed, cannot be explained by current stellar models. Other physical mechanisms, such as stellar rotation, should be investigated in the future. More observations in open clusters of various ages (and thus turn-off masses) are also required to increase the small number statistic of this study.

The oxygen abundance is very deficient (by 0.2 to 0.5 dex depending on the true gf value of the Ni I $\lambda 6300.34$ line) relative to iron in all our four red giants for which the oxygen abundance could be measured. This is not compatible with stellar model calculations which predict an oxygen deficiency by at most 0.03 dex after the first dredge-up. The high deficiencies can be partly explained if we assume that the Sun is slightly oxygen-rich relative to most stars in its neighborhood, as suggested by several authors. If not, then a new mechanism in stellar models should be thought of to account for this discrepancy.

Acknowledgements. We thank Dr. Pierre Dubath for his help with the INTER-TACOS software used for the reduction of echelle spectra, and Dr. Laura Fullton for providing us with Dr. Sneden's ftp address from which we downloaded the MOOG code. PN thanks Dr. Georges Meynet for a fruitful discussion. This work was supported in part by the Swiss National Science Foundation.

References

Arnould M., Goriely S., Jorissen A., 1999, A&A 347, 572
Bell R.A., Eriksson K., Gustafsson B., Nordlund A., 1976, A&AS 23, 37
Becker W., Svolopoulos S.N., Fang Ch., 1976, Kataloge photographischer und photoelektrischer Helligkeiten von 25 galaktischen Sternhaufen im RGU- und U$_c$BV-System. Univ. Basel
Bessel M.S., Castelli F., Plez B., 1998, A&A 333, 231
Biémont E., Karner C., Meyer G., Träger F., zu Putlitz G., 1982, A&A 107, 166
Boyarchuk A.A., Aantipova L.I., Boyarchuk M.E., Savanov I.S., 1996, Astronomy Reports 40, 783
Brown J.A., Wallerstein G., 1991, AJ 101, 1693
Canuto V.M., Goldman I., Mazzitelli I., 1996, ApJ 473, 550
Edvardsson B., Andersen J., Gustafsson B., et al., 1993, A&A 275, 101
Eggen O.J., 1968, ApJ 152, 83
Flower P.J., 1977, A&A 54, 31
Gratton R.G., Carretta E., Eriksson K., Gustafsson B., 1999, A&A 350, 955
Grevesse N., Noels A., 1993, In: Hauck B., Paltani S., Raboud D. (eds.) La formation des éléments. 35e Cours de perfectionnement de l'AVCP, p. 205
Kurucz R.L., 1994, Kurucz CD-ROM 20-22

Kurucz R.L., 1996, Kurucz CD-ROMs 24 and 25
Lambert D.L., 1978, MNRAS 182, 249
Luck R.E., 1994, ApJS 91, 309
Maeder A., Meynet G., 1991, A&AS 89, 451
Mermillod J.-C., 1995, In: Egret D., Albrecht M.A. (eds.) Information & on-line data in astronomy. Kluwer, p. 127
Mermillod J.-C., 1999, In: Rebolo R. (ed.) Very low-mass stars and brown dwarfs. Cambridge University Press, in press (see also http://obswwww.unige.ch/webda)
Mermillod J.-C., Mayor M., 1989, A&A 219, 125
Mermillod J.-C., Mayor M., 1990, A&A 237, 61
Mowlavi N., 1998, In: Cosmic chemical evolution. IAU Symp. No 187, in press
Mowlavi N., 1999, A&A 350, 73
Piskunov N.E., Kupka F., Ryabchikova T.A., Weiss W.W., Jeffery C.S., 1995, A&A 112, 525
Schaller G., Schaerer D., Maeder A., Meynet G., 1992, A&AS 96, 269
Strobel D., 1991, Astron. Nachr. 312, 177
Takeda Y., Takada-Hidai M., 1994, PASJ 46, 395
Thévenin F., 1989, A&AS 77, 137
Thévenin F., 1990, A&AS 82, 179
Twarog B.A., Ashman K.M., Anthony-Twarog B.J., 1997, AJ 114, 2556
Udry S., Mayor M., Maurice E., et al., 1999, In: Hearnshaw J.B., Scarfe C.D. (eds.) Precise stellar radial velocities. IAU Symp. 170, ASP Conf. Series Vol. 185, p. 383
Venn K.A., 1999, ApJ 518, 405
Wiese W.L., Smith M.W., Miles B.M., 1969, NSRDS-NBS 22, Vol. II